Final Technical Report
AFOSR Grant No. F49620-01-1-0074

Mathematical and Computational Framework for Virtual Fabrication Environment for Aircraft Components

Barna Szabó[1], Sebastian Nervi[2] and Daniel Muntges[3]
Center for Computational Mechanics
Washington University, Campus Box 1129
one Brookings Drive
St. Louis, MO 63130-4899

Acknowledgements

This work was sponsored by the Air Force Office of Scientific Research, Air Force Materiel Command, USAF, under grant number F49620-01-1-0074. Valuable experimental data were provided by the Metallic Processes and Prototyping Laboratory of Boeing Phantom Works, St. Louis, Alcoa Technical Center, Los Alamos National Laboratory and Oak Ridge National Laboratory. X-ray diffraction measurements were performed at WPAFB.

Dr. David M. Bowden, Technical Fellow, Advanced Manufacturing Research & Development, Mr. Keith Young, Engineer/Scientist, Metallic Processes and Prototyping Laboratory, Boeing Phantom Works, St. Louis, Dr. Mark Newborn, Alcoa Technical Center, Dr. Michael B. Prime, Technical Staff Member, Los Alamos National Laboratory provided advice and assistance in this investigation.

Disclaimer

The views and conclusions contained herein are those of the authors and should not be interpreted as necessarily representing the official policies or endorsements, either expressed or implied, of the Air Force Office of Scientific Research or the U.S. Government.

[1]The Albert P. and Blanche Y. Greensfelder Professor of Mechanics.
[2]Graduate Research Assistant.
[3]Graduate Research Assistant.

Contents

1 Summary

This project addressed some fundamental questions that pertain to the utility of the methods of numerical mathematics in engineering decision-making processes. The basic methodology investigated concerns the problem of selection, calibration and validation of mathematical models and thus transcends particular applications. The principal objective was to perform an investigation on the development of cost-effective methods for the design and analysis of unitized metallic airframe components that account for the effects of residual stresses and provide sufficiently reliable information to serve as a basis for certification or rejection of manufactured components.

1.1 Air Force relevance

This project addressed some of the key requirements identified in the report Uninhabited Air Vehicles: Enabling Science for Military Systems (2000) National Materials Advisory Board, Aeronautics and Space Engineering Board [1]. The following statements are quoted from the referenced report:

Analytical tools

"Research should be initiated to integrate design and analysis models and methods into a versatile engineering tool. Current analytical models, such as the finite element codes developed by the National Aeronautics and Space Administration (NASA) and structural evaluation codes developed by industry, will have to be modified and improved for structural design and analysis in a production environment. The development of analytical tools should also include the development of procedures for assessing the accuracy and reliability of model predictions." (p. 52)

Characterization and Testing

"Fundamental research should be undertaken to establish potential failure modes and performance levels for materials and structures to support probabilistic analysis methods. Current approaches for testing materials are based on deterministic design methods and rely on extensive testing at the subelement, element, subcomponent, component, and full-scale levels, using a building block approach (NRC, 1996). The development of basic property relationships and potential failure modes are needed for implementing probabilistic design approaches and reducing the amount of large-scale verification testing required." (p. 53)

Simulation Methods

"Techniques and software codes should be developed for computational simulations of structural responses to operational environments throughout the structures lifetime at both the

material and structural levels. Effective analytical simulations would enable designers to model design alternatives without developing and testing expensive prototypes, resulting in potentially significant reductions in developmental costs." (p. 53)

Design Criteria

"Fundamental research on critical failure modes and property relationships to establish meaningful design criteria for probabilistic methods should be undertaken. Criteria could be established based on the results of studies on the relationship between the conventional safety factor and the probabilistic reliability of a structure, along with an in-depth survey of existing structures." (p. 53)

Recommendation

"To support the development and introduction of probabilistic methods for UAVs, the U.S. Air Force should sponsor research on (1) analytical tools, (2) characterization and testing, (3) simulation methods, and (4) design criteria." (p. 53)

While reference [1] addressed design needs associated with the development of UAVs, a software product that will meet its recommendations will have a much broader applicability in both the military and civilian sectors: The value of information acquired through various applications of the techniques of numerical mathematics is strongly correlated with its reliability. Reliable information will serve to reduce product cycle costs, whereas engineering decisions based on unreliable information are more than likely to cause costly problems. Unreliable information has a negative economic value: Having misleading information is worse than knowing that some information is unavailable.

It is well known that finding problems late in a product cycle is generally very expensive in terms of costs and performance. The failure of the C-17 wing in a static test in October 1992 is a case in point [2]. The costs of repair, retrofitting and weight penalties typically can be traced to erroneous decisions made in the design phase.

The key to improved reliability in numerical simulation is systematic application of two complementary processes called verification and validation (V&V). Verification is concerned with proper approximation of the exact solution of a mathematical model, called working model. The goal of verification is to ensure that the exact solution is approximated with sufficient precision, so that decisions based on data computed from the approximate solution are substantially the same as decisions based on data that would be computed from the exact solution. Validation is concerned with proper selection of the working model. The goal of validation is to ensure that simplifying assumptions incorporated in the working model do not affect the data of interest significantly. A more detailed discussion on V&V is presented in Section 2.

With very few exceptions, V&V processes are not used in current practice and hence the full potential of computer-aided engineering (CAE) technology is not being realized. The consequences are erroneous and sub-optimal engineering decisions, unnecessary and poorly

conceived physical experimentation, long product cycles and costly maintenance. This very important aspect of numerical mathematics is receiving an increasing amount of attention in computational fluid dynamics (CFD) (see, for example, [3], [4], [6], [5]) but has not yet received much attention in solid mechanics.

This project illustrates the benefits that can be derived from the application of V&V processes to thin-walled unitized structural components manufactured by means of high-speed machining (HSM) techniques. A test article, typical in complexity of unitized structural components, is shown in Fig. 1.

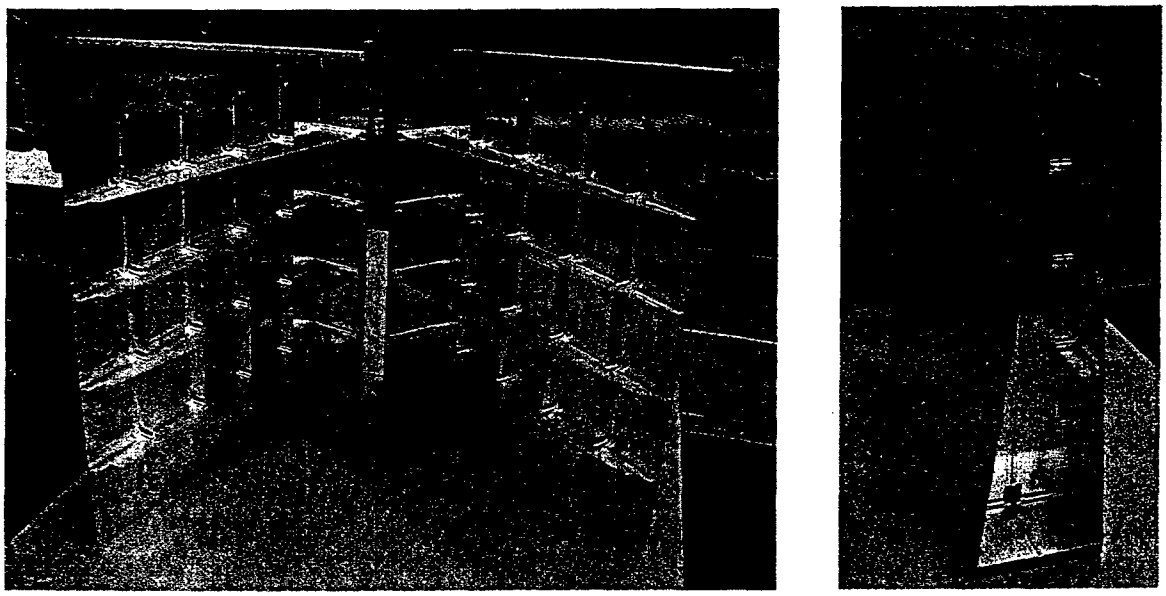

Figure 1: Test article for gridlock experiments. Some of the panels are buckled by residual stresses. Reproduced with permission from The Boeing Company.

There are strong economic incentives for increasing material utilization factors, reducing machining times and increasing the success rate for machining unitized structural components, such as spars, keel beams, bulkheads[4]. A reliable virtual fabrication environment is essential for controlling the costs associated with fabrication of complex aircraft components and improving the quality of the design process.

There is a need for specialized software products that provide in-depth simulation capabilities for specific classes of problems. This project exemplifies a new paradigm in numerical simulation and with reference to an important problem class: the design and certification of unitized metallic airframe components.

[4]Economic estimates have been developed by Dr. David M. Bowden, Technical Fellow, The Boeing Company, St. Louis, MO 63166 Tel. 314-232-1859, david.m.bowden@boeing.com.

1.2 Objectives

The objectives of this project were in two categories: General objectives and specific, goal-oriented objectives:

1.2.1 General objectives

One of the fundamental questions of numerical mathematics is how mathematical problems should be formulated so that they can serve as reliable and accurate representations of physical reality. A well-constructed mathematical model should provide predictions of events or states of systems that can be confirmed consistently by physical observations.

The general objective was to develop guidelines for the development of working models for the simulation of the structural and strength responses of unitized aircraft components and interpretation of physical experiments based on V&V procedures.

1.2.2 Specific objectives

The specific objectives were to investigate the application of V&V procedures to the solution of specific engineering problems of substantial significance in aerospace engineering. This requires access to carefully developed experimental data, Based on the availability of experimental data, two areas were selected for detailed investigation:

1. Development of the mathematical and computational aspects of the knowledge base needed for the creation of a virtual fabrication environment for light weight aircraft and spacecraft components manufactured from 7050-T7451 aluminum plate stock that will make it possible to plan the fabrication processes so that the incidence of re-working and scrapping of partially or fully manufactured parts is substantially reduced.
2. Investigation of working models for the analysis of thin-walled structural components fabricated by mechanical milling.

1.3 Accomplishments

The main accomplishments are summarized in relation to the general and specific objectives in the following.

1.3.1 General objectives

The formulation of rules for design and fabrication generally involves evaluation of experimental data with the objective to test whether a working model or hypothesis concerning material properties, failure criteria or boundary conditions, should be accepted or rejected. There are three sources of error: (a) errors in the working model or hypothesis being tested, (b) errors in the numerical approximation and (c) errors in the experiment. Unless the errors

in the experiment and the numerical approximation are controlled, it will not be possible to judge whether the working model or hypothesis should be rejected or not.

1. Destructive physical experiments, performed with the objective to determine residual stresses, involve measurements of strains and displacements in specific locations. The distribution of the residual stress is inferred from the observations by numerical means, using a working model based on the assumption that the residual stress state depends only on the initial stress distribution and the current configuration of the body. This assumption had not been proven, however. A proof was developed under this project.

2. Working models used for the purpose of interpretation of layer removal experiments are typically based on the assumption of plane strain conditions. In reality, however, the conditions under which these experiments are performed are more closely approximated by generalized plane strain than plane strain conditions. The errors in the working model associated with the use of plane strain rather than generalized plane strain conditions were estimated by theoretical and numerical means.

3. The choice of a working model is based on expert opinion formulated with the aid of virtual and physical experimentation. It was shown that in many cases the use of virtual experimentation has advantages over physical experimentation.

1.3.2 Specific objectives

1. Physical experiments were performed and independently obtained experimental data, provided by Los Alamos National Laboratory, were analyzed in an effort to determine residual stresses induced by the manufacturing process of 2 to 4-inch 7050-T7451 aluminum plate stock. The experimental arrangement is shown in Fig. 2.

2. The distortion of thin-walled test articles typical of unitized aircraft components made of 7050-T7451 aluminum was predicted. A working model incorporating the assumptions of the linear theory of elasticity was used for this purpose. The results indicated that the magnitude of distortion that can be attributed to the residual stresses caused by the manufacturing process of 7050-T7451 plate stock is not substantial. Consequently, either the working model is not suitable for the intended purpose, or the large distortions observed in manufacturing are caused by machining-induced stresses. In order to determine the reason for the differences, validation experiments had to be performed.

3. Validation experiments were performed with the objective to identify the effects of the bulk stresses (the stresses caused by the manufacturing process of the plate). The results were consistent with 'blind' predictions based on the working model. Since machining-induced stresses can be removed by chemical milling, the results indicate that high-speed machining should be used for the fabrication of unitized aircraft components from 7050-T7451 aluminum plate stock to slightly larger then the intended dimensions, then chemical milling should be used to obtain the final dimensions.

4. Experimental data obtained for intersecting thin-walled cylindrical shells was analyzed, utilizing a hierarchic modeling concept. It was concluded that in the case of thin-walled components, subjected to loads in the linearly elastic range, complicated physical experiments are not warranted. Virtual experimentation is sufficient for the purposes of strength analysis of such components.

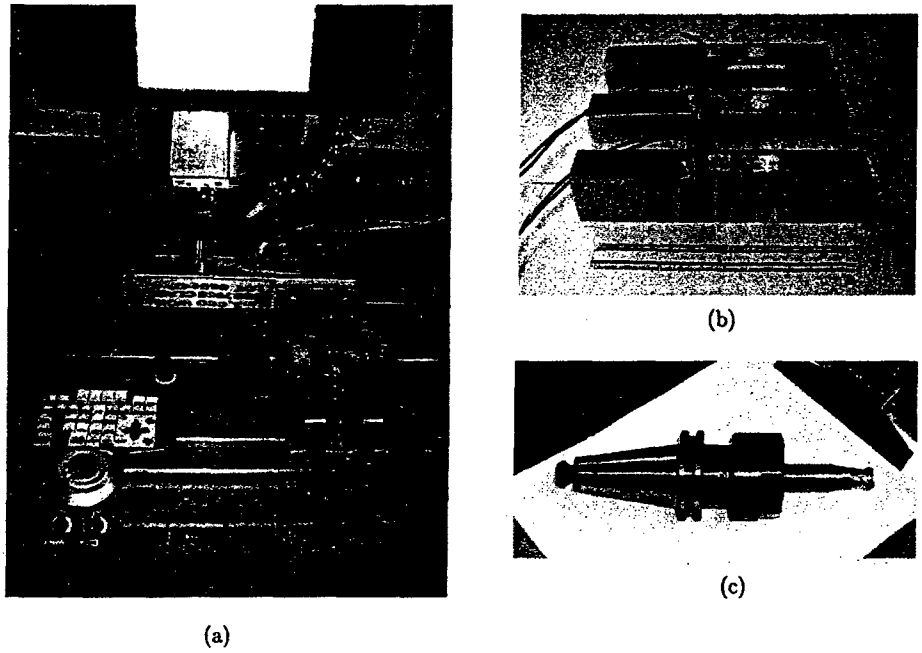

(a) (b) (c)

Figure 2: Experiments performed at Washington University. (a) The milling machine and controls (Cincinnati Milarcon Sabre machining Centre). (b) Instrumented specimens. (c) The milling tool: 3/4 inch end mill (two flutes) corner radius: 0.120 inches (3.05 mm).

1.4 Archived Publications

The following papers and theses that document various aspects of this effort have either been published or are in the process of being published:

Szabó B and Actis R. On the importance and uses of feedback information in FEA, *Applied Numerical Mathematics.* 52 (2005) 219-234.

Szabó B, Düster A and Rank E. The p-version of the finite element method. In: E. Stein, R. de Borst, T.J.R. Hughes (Eds.) *Encyclopedia of Computational Mechanics.* Vol. 1, Fundamentals, Ch. 5. John Wiley & Sons, London 2004.

Babuška I and Szabó B. On the generalized plane strain problem in thermoelasticity. Submitted to *Comput. Methods Appl. Mech. Engng.* Under review.

Szabó B and Muntges D. Procedures for the verification and validation of working models for structural shells. Journal of Applied Mechanics. Paper No. JAM-04-1223. In press.

An extended version of this paper is available in the Proceedings, 2004 ASME International Mechanical Engineering Congress, Anaheim, CA Paper No. IMECE2004-60014 November 2004.

Liebschutz RI. Simulation of residual stresses in aluminum alloy using p-version finite element methods. MS Thesis, Washington University, June 2002.

Muntges D. Verification and validation of working models for thin cylindrical shells. MS thesis, The Henry Edwin Sever Graduate School, Washington University, St. Louis, December 2004.

Nervi S. A mathematical model for the estimation of the effects of residual stresses in aluminum plates. D.Sc. Thesis, Washington University, May 2005.

2 Verification and validation

The statement: *" Effective analytical simulations would enable designers to model design alternatives without developing and testing expensive prototypes, resulting in potentially significant reductions in developmental costs."* in reference [1] emphasizes the desirability of replacement of physical testing programs with numerical simulation. This is possible if the numerical simulation methods are sufficiently reliable. In this section the problem of quality assurance in numerical simulation is discussed.

The main elements of numerical simulation and the associated errors are illustrated schematically in Fig. 3. The goal of CAE is to obtain reliable quantitative information concerning some physical system. To achieve this goal, a working model has to be defined and a numerical solution obtained. These points are discussed in the following sections.

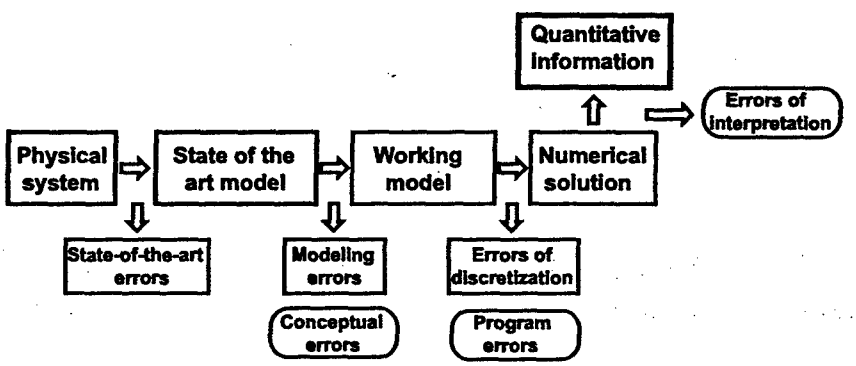

Figure 3: The main elements of numerical simulation and the associated errors.

2.1 State of the art models

The fullest possible mathematical representation of a physical system or object, utilizing state of the art methods and information, is called a state of the art model. State of the art models are generally very complicated and the information sought usually can be acquired with simpler models. For these reasons simplified models, called working models, are formulated.

2.2 Working models

Working models are mathematical problems formulated with the objective to capture the essential characteristics of state of the art models with the expectation that engineering conclusions based on them will be substantially the same as if the state of the art model had been used.

Associated with each working model is a modeling error (indicated schematically in Fig. 3). At present the selection of a working model, and hence the control of modeling errors, is largely left to the experience and judgment of analysts and designers. However,

as the complexity of the systems increases, reliance on experience and judgment becomes increasingly impractical. Expert knowledge must be aided by virtual and physical experimentation. Selection of the appropriate working model for a given problem is the most important decision in any CAE application.

Evaluation and modification of a working model through virtual and physical experimentation and correlation of computed information with experimental data is called validation. The goal of validation is to ensure that the model is a sufficiently accurate mathematical description of the physical system or process it is supposed to represent [3], [4], [6]. Validation involves calibration and prediction. The determination of physical properties and other model parameters through correlation with experiments is called calibration. The use of a model to foretell the state of a physical system under conditions for which the model has not been calibrated is called prediction.

It is important to note that successful prediction of the outcome of one or more physical experiments does not prove that the working model will provide correct predictions for other experiments or applications. It shows only that the working model meets necessary conditions for acceptance. The reliability of working models can be established to a high degree of certainty only through carefully designed validation experiments [4], [6].

2.3 Numerical solution

The solution of a working model is approximated by numerical means, most frequently by the finite element method (FEM) [7]. It is necessary to ensure that the data of interest computed by numerical means are within acceptable error bounds with respect to their counterparts corresponding to the exact solution of the working model.

Determination of the accuracy of data computed from the approximate solution of a particular mathematical model is called verification. In a verification process accuracy is understood to be with respect to the exact solution of the working model, not with respect to physical reality. In the terminology introduced in Fig. 3, verification is concerned with estimation and control of the errors of approximation and determination that the program is functioning as intended by the developer.

2.4 Reliability of computed information

Information generated by numerical means will be reliable only if the state-of-the-art errors, the modeling errors and the errors of approximation are sufficiently small and no conceptual errors, or errors of interpretation, or programming errors have occurred. Proper selection of a working model depends on the goals of computation. Commonly occurring conceptual errors include attempting to compute data that are inconsistent with the formulation of the working model. The detection of programming errors is usually quite difficult, necessitating careful checking of the program for the problem class and the data of interest.

The state of the art errors, the modeling errors and the errors of approximation are

benign errors in the sense that these are controllable errors. State-of-the-art errors can be reduced by experimentation; modeling errors and errors of discretization can be reduced by automated or user-guided adaptive processes. Conceptual errors, errors of interpretation and programming errors are malignant, in the sense that they render the results of analysis useless, or worse, misleading.

2.5 Why is numerical accuracy important?

It is often asked: *"If we do not know the loading data with sufficient accuracy then why do we need to be concerned with the accuracy of the numerical solution?"* In answering this question we consider two important areas: The application of design rules and formulation of design rules. It is shown in the following that neither proper formulation nor proper application of design rules is possible without estimation and control of the numerical accuracy.

2.5.1 Formulation of design rules

The formulation of design rules involves evaluation of experimental data with the objective to test whether a working model or hypothesis concerning material properties or failure criteria should be accepted or rejected. There are three sources of error: (a) errors in the working model or hypothesis being tested, (b) errors in the numerical approximation and (c) errors in the experiment. Unless the errors in the experiment and the numerical approximation are controlled, it will not be possible to judge whether the working model or hypothesis should be rejected or not.

2.5.2 Application of design rules

Design and design certification involve application of existing design rules, established by various codes and conventions of professional practice. The design conditions and criteria to be used are mandated by the cognizant authorities. There is no uncertainty concerning the loading conditions or other types of excitation that must be considered, or the physical properties to be used. The design rules are typically stated in the form of required minimum factors of safety (FS):

$$FS := \frac{\Phi_{\text{lim}}}{\Phi_{\text{max}}(u_{EX})} \tag{1}$$

where $\Phi_{\text{lim}} > 0$ is the limiting (not to exceed) value of some functional (such as maximum stress) and $\Phi_{\text{max}}(u_{EX}) > 0$ is the exact value of the same functional corresponding to the exact solution of the mathematical model. The designer's responsibility is to ensure that the applicable design rules are followed.

We will denote by $\Phi_{\text{max}}(u_{FE})$ the value of Φ_{max} computed from the finite element solution. Let us suppose that, owing to numerical errors, it is possible to guarantee only that the

relative error is less than τ:

$$\frac{|\Phi_{\max}(u_{EX}) - \Phi_{\max}(u_{FE})|}{\Phi_{\max}(u_{EX})} \leq \tau \quad 0 \leq \tau < 1$$

i.e., $\Phi_{\max}(u_{FE})$ may underestimate $\Phi_{\max}(u_{EX})$ by 100τ percent. Therefore we have:

$$\Phi_{\max}(u_{EX}) \leq \frac{1}{(1-\tau)}\Phi_{\max}(u_{FE})$$

on substituting this expression into eq. (1), we have:

$$FS \leq (1-\tau)\frac{\Phi_{\lim}}{\Phi_{\max}(u_{FE})}. \tag{2}$$

Denoting the factor of safety to be used in conjunction with the data generated by finite element analysis by FS_{FE}:

$$FS_{FE} := \frac{\Phi_{\lim}}{\Phi_{\max}(u_{FE})}$$

we have from eq. (2):

$$FS_{FE} \geq \frac{FS}{1-\tau}. \tag{3}$$

This result shows that to compensate for numerical errors in the computation of $\Phi_{\max}(u_{FE})$, it is necessary to increase the required factor of safety to $FS/(1-\tau)$. For example, if the accuracy of $\Phi_{\max}(u_{FE})$ can be guaranteed to 20% (i.e., $\tau = 0.20$) then the factor of safety must be increased by 25% to compensate for numerical errors. Since the factor of safety was already chosen conservatively to account for various uncertainties, the economic penalties associated with using an increased factor of safety generally far outweigh the costs associated with guaranteeing the accuracy of the data of interest to within a small relative error (say 5%).

It is necessary to specify the acceptable error tolerance in numerical analysis and to verify that the error is not larger than the specified tolerance even when that tolerance is large.

2.6 Aspects of implementation

In the early papers and books on finite element analysis it was customary to write strain in the following form

$$\{\epsilon\} = [D][N]\{a\} = [B]\{a\}$$

where $[N]$ is the matrix of element-level basis functions and $\{a\}$ are the coefficients of the basis functions (see, for example [10], [11]). Therefore the element-level stiffness matrix was written as:

$$[K_e] = \int_{\Omega_e} [B]^T [E][B]\, dV$$

rather than in the form:

$$[K_e] = \int_{\Omega_e} ([D][N])^T [E][D][N]\, dV.$$

In this way the formulation of the working model, represented by the operator [D], the polynomial degree of the elements and the mapping functions which are related to discretization, were combined. This lead to the development of large element libraries with separate element types for each working model and polynomial degree, such as the constant strain triangle, the Argyris triangle, Bell's triangle, Hsieh-Clough-Tocher triangle for plate bending (a description and analysis of which is available in [13]), various shallow shell elements, etc. There are elements in commercial computer codes for which the details of the formulation are not made available. The infrastructures of these codes were designed to support control of discretization errors through mesh refinement, using elements of fixed and low polynomial degree, but do not provide for systematic control of modeling errors. For a discussion on shell elements we refer to [12].

In the hierarchical view the formulation and the discretization must be separated in order to provide a suitable computational framework for selecting a suitable working model and for verifying the computed information. Furthermore, working models must be defined so that they have consistent meaning when passing from one model to another.

Considering control of discretization errors, once again a hierarchic framework is needed. The goal of computation is to approximate some functionals $\Phi_i(u_{EX})$, $i = 1, 2, \ldots$, to within a specified tolerance. Of course, the exact solution is generally not known, however certain properties of the exact solution are known a priori. It is necessary to construct a sequence of finite element spaces $S_1(\Omega) \subset S_2(\Omega) \subset \cdots \subset S_k(\Omega) \subset \cdots$ and compute the corresponding finite element solutions $u_{FE}^{(k)}$ and from the finite element solutions the functionals $\Phi_i(u_{FE}^{(k)})$, $k = 1, 2, \ldots$ This has very substantial impact on the design of an implementation. Conventional implementations were not designed in this way. For this reason they are not suited well for systematic control of the errors of idealization or the errors of discretization.

3 Residual stresses

In this section we address the specific objective of developing a model that can predict, with reasonably accuracy, the distortion of a part machined from large metal plates, in particular from 50.8 mm (2 in) to 101.6 mm (4 in) thick 7050-T7451 aluminum plates, caused by residual stress introduced in the manufacturing process of the plates. The pattern of residual stress in this aluminum plate is complicated because following quenching, the plates are stretched in order to reduce the magnitude of residual stresses. Since the data that characterize the yield behavior of the material vary through the thickness, a complicated pattern of residual stress develops, which is illustrated in Fig. 5.

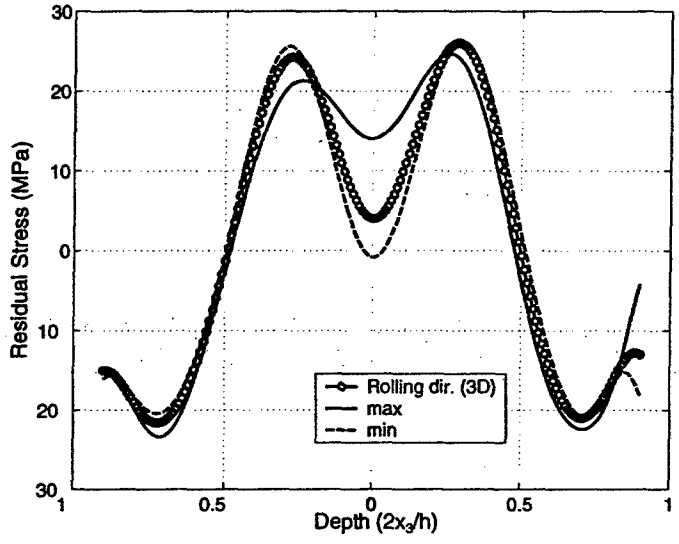

Figure 4: Residual stress distribution in the transverse direction.

The determination of residual stresses is by destructive experiments. In these experiments displacements and/or strains are measured from which the residual stress state is inferred. The experimental arrangement for the determination of residual stresses by the wide slot method is shown in Fig. 2. The underlying theory is based on the assumption that the principle of superposition holds, from which the property of path independence, discussed in the following section, can be proven.

3.1 Path independence

Let us denote the initial domain of a body by Ω_0, its boundary points by $\partial\Omega_0$ and the initial stress state by σ^0_{ij}. The initial stress state satisfies the equations of equilibrium $\sigma^0_{ij,j} = 0$ on Ω_0 and the stress-free boundary conditions, i.e. $\sigma^0_{ij} n_j = 0$ on $\partial\Omega_0$ where n_j is the unit normal.

Let us now introduce a cut Γ_1, that produces the domain Ω_1, and a second cut Γ_2 to

produce a domain Ω_2. Denote the displacement field following the first (resp. the second) cut by U_i^1 (resp. U_i^2). The notation is shown in Fig. 5.

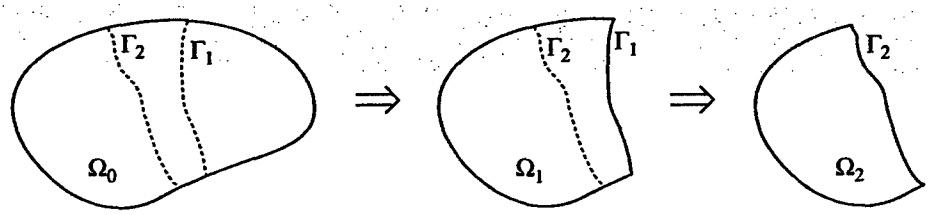

Figure 5: Path independence. Notation.

Theorem 3.1 U_i^2 depends on σ_{ij}^0 and Ω_2 but not on U_i^1 or Ω_1.

Proof: U_i^1 satisfies

$$B(U_i^1, v_i) = -\int_{\Gamma_1} \sigma_{ij}^0 n_j v_i \, dS \qquad \forall \, v_i \in E(\Omega_1) \tag{4}$$

where $B(U_i^1, v_i)$ is the bilinear form corresponding to the principle of virtual work, v_i is a test function and $E(\Omega_1)$ is the energy space.

Denote by S_{ij}^1 the stress field corresponding to U_i^1 on Ω_1 and let u_i^2 be the displacement field on Ω_2 corresponding to the tractions $S_{ij}^1 n_j$ acting on Γ_2, therefore

$$B(u_i^2, v_i) = \int_{\Gamma_2} S_{ij}^1 n_j v_i \, dS \qquad \forall \, v_i \in E(\Omega_2). \tag{5}$$

The displacement field corresponding to the second cut is $U_i^2 = u_i^2 + \tilde{U}_i^2$, where

$$B(\tilde{U}_i^2, v_i) = -\int_{\Gamma_2} (\sigma_{ij}^0 + S_{ij}^1 n_j) v_i \, dS \qquad \forall \, v_i \in E(\Omega_2). \tag{6}$$

Adding eq. (5) and eq. (6) we find that

$$B(U_i^2, v_i) = -\int_{\Gamma_2} \sigma_{ij}^0 n_j v_i \, dS \qquad \forall \, v_i \in E(\Omega_2) \tag{7}$$

which proves the theorem.

Remark 3.1 Here we have considered an unconstrained body, hence the displacements are understood to be displacements up to rigid body displacements. Of course, a part cannot be machined without constraints. However, if the effect of the constraints is elastic, and the constraint conditions do not change during the machining process, then the result obtained in eq. (6) remains unchanged, therefore Theorem 3.1 holds under these conditions also.

Remark 3.2 We have assumed that when the body is cut, the cutting operation will not introduce stresses. However in mechanical milling additional residual stresses are introduced. The magnitude of these stresses are substantial only in a thin layer near the surface. This problem is discussed in the following section.

3.2 Validation experiments

Validation experiments were performed at the Metallic Processes and Prototyping Laboratory of Boeing Phantom Works, St. Louis. The objective of the experiments was to test whether the linear working model meets necessary criteria for acceptance. The working model is based on the assumption that if the stresses introduced by the machining process were negligibly small then, in accordance with Theorem 1, the configuration of a workpiece after machining is predictable from the shape of the part and the residual stress distribution in the plate from which it was machined.

The validation experiments were planned jointly by the research groups at the Center for Computational Mechanics of Washington University and Boeing Phantom Works in St. Louis. A detailed description of the experimental procedure is available in [9]. It was decided to machine four test articles having a Z-shaped cross-section from a single 4 inch (101.6 mm) thick 7050-T7451 aluminum plate. The nominal dimensions of the test articles are shown in Fig. 6. The thicknesses of the test articles ranged from 0.04 to 0.12 inches. In addition, test specimens were cut from the same plate and the residual stresses were determined by the wide slot method [8]. These experiments were similar to those performed at Washington University earlier.

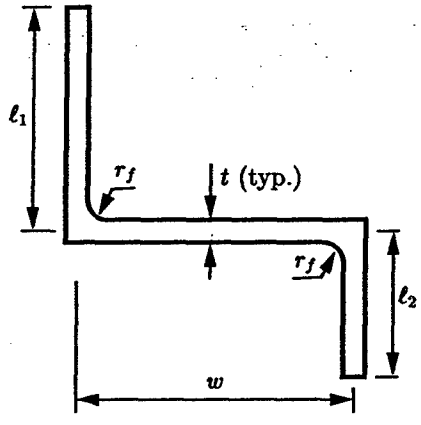

NOMINAL DIMENSIONS

Dimension	mm	inches
Thickness t_1	3.048	0.12
Thickness t_2	2.032	0.08
Thickness t_3	1.524	0.06
Thickness t_4	1.016	0.04
Flange width ℓ_1	40.64	1.60
Flange width ℓ_2	25.4	1.00
Web w	50.8	2.00
Fillet radius r_f	3.048	0.12
Length L	914.4	36.00

Figure 6: Cross-section and nominal dimensions of the test articles.

Some machining-induced stresses are invariably present following mechanical milling operations. Based on existing experimental evidence it is expected that the machining-induced stresses are confined to within a small layer at the surface of the material and therefore their effects on distortion would increase as the thickness of the test articles decreased.

Machining-induced stresses can be eliminated by chemical milling. Assuming that the principle of superposition holds, and the data obtained for the aluminum plate are reliable, it should be possible to predict the deformed configuration of a test article once the machining-induced stresses were removed. Referring to Fig. 6, the two specimens of thicknesses t_1 and t_2 were chemically milled to thicknesses t_3 and t_4 in an effort to eliminate the residual stresses introduced by the machining process and to have a direct comparison between the configurations of test articles of the same thickness, one of which is affected by the machining-

induced stresses, the other is not. The four Z-shaped test articles attached to the plate by thin tabs, are shown in Fig. 7.

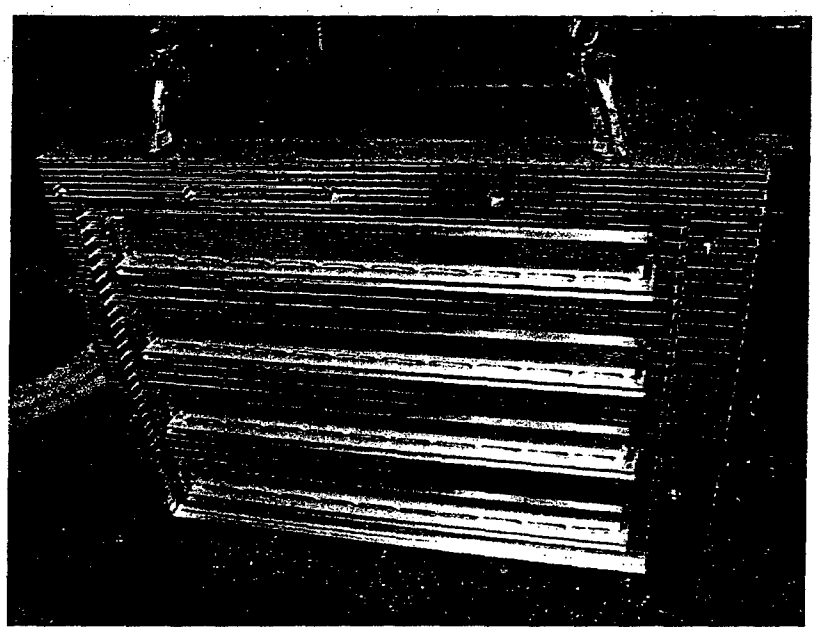

Figure 7: The four Z-shaped test articles after machining. The test articles are supported by tabs.

The working model proposed for predicting the distortion caused by bulk stresses was solved numerically using the finite element method, and the solution was verified using hierarchic sequences of finite element spaces. The model was tested with the objective to determine whether it meets necessary conditions for acceptance. This test involved correlation with experiments using a 'blind' prediction: The analyst (S. Nervi) made the prediction without having seen the outcome of the experiments and the person conducting the experiments (K. Young) was not aware of the predicted configuration.

The configuration of the Z-shaped test articles was measured following mechanical and chemical milling on three faces using a contact probe with a measurement error of ± 0.0127 mm (± 0.0005 in). The measured data were adjusted to ensure that the same coordinate system was used in measuring the configurations prior to and following chemical milling.

3.3 Sources of error and uncertainty

When comparing the results of physical experiments with data obtained by numerical simulation, it is necessary to consider the differences between the real physical object and its mathematical description.

3.3.1 Thickness variation

In the mathematical model uniform thickness was assumed. In the test articles there were small variations in thickness that lead to variations in the displacement field.

3.3.2 Variation of residual stress over the plate

The wide slot method used for obtaining the bulk stresses has inherent sources of error and uncertainties, such as the effect of the machining-induced stresses caused by the cutting tool used for creating the slot, and the error associated with the measured strains which will lead to errors in the computed value of the bulk stresses. Furthermore, the bulk stresses were obtained from samples taken from a different location than the test articles and it was assumed that the bulk stresses were uniform over the plate. Since we considered a linear material law, variations in the magnitude of the residual stresses will lead to similar variations in the magnitude of the predicted distortion.

3.3.3 Material properties

The material properties used were standard values, no experiments were conducted to determine the modulus of elasticity (E) and Poisson's ration (ν). The method used for computing the residual stresses is based on a linear material law for which the computed residual stresses will "adjust" any actual difference between the real value and the value used in the numerical simulation. Therefore, differences between the actual values of the material properties and the ones used in the simulations will not affect the computed distortion but they will affect the computed residual stress after material removal.

3.3.4 Measurement errors

The configuration of the test articles was measured by supporting each test article in three points using spherical contact probes. The test articles were bonded to the contact probes. The coordinates were measured using an automated contact probe, which approached the test article along the normal to its surface until contact was made. Since contact is necessary in order to obtain a measurement, the probe could affect the displacement when the test article is thin. Furthermore, the effect of gravity, not considered in the numerical simulation, could also have a small effect on the configuration of the test articles.

3.4 Results

The distortion of the test articles increased with decreasing thickness. This is consistent with the expectation that the effects machining-induced stress are strongly correlated with thickness.

The predicted and measured configurations of the chemically milled test articles were very similar and substantially different from the configuration of test articles that were not milled chemically. The predicted distortion was somewhat smaller than the observed distortion. This can be explained by the differences between the test articles and their mathematical representation, the variations in thickness are likely to be the main reason for the differences. Details are available in [8].

4 Models for intersecting shells

In structural shells, such as pressure vessels and piping systems, there are regions where the kinematic assumptions incorporated in classical shell models do not hold. These are the neighborhoods of nozzles and shell intersections, support attachments, stiffeners, cut-outs, and regions where the curvature abruptly changes. From the point of view of engineering design and analysis, these are the typical regions of primary interest, however.

In formulating mathematical models, shell-like structures should be viewed as fully three-dimensional solid bodies that allow the imposition of restrictions on the transverse variation of displacement vector components in certain regions. The imposition of such restrictions reduces a three-dimensional problem to a two-dimensional one in the case of plates and shells; to a one-dimensional problem in the case of beams and arches. An important practical problem is to identify the proper formulation for a particular application, that is, a formulation that simplifies the problem by dimensional reduction without affecting the data of interest significantly.

In our terminology a working model is a mathematical model of some physical system or process comprised of a formulation and data pertaining to geometric description, material properties, loading and constraints. Associated with a working model is an exact solution.

Common to all mathematical models based on the principles of continuum mechanics are the conservation of momentum (in static problems the equations of equilibrium), the strain-displacement relations and constitutive laws. A particular application involves selection of a working model.

Any working model should be viewed as a special case of a general model, called state of the art model. By definition, a state of the art model accounts for all physical laws that pertain to the system or process being modeled. Selection of a particular working model involves acceptance of certain limitations that may or may not be justified, given the goals of computation. In general it is not known a priori whether the limitations of a particular working model are justified. Therefore it is necessary to perform tests a posteriori to determine whether a particular working model is suitable with respect to the goals of computation. If the tests show that a working model is inadequate then a more comprehensive working model must be chosen and the process repeated.

In principle, one could continue this process indefinitely until all relevant attributes of the physical system or process being modeled are taken into account. In reality however the more comprehensive a working model, the more descriptive data that characterize the geometric description, material properties and boundary conditions are needed. Often the needed parameters are not available, or would be difficult to determine. The cognitive as well as the stochastic uncertainties increase with the complexity of the working model. Therefore a highly detailed working model is generally not feasible. Consequently is some degree of uncertainty associated with any attempt to model a physical system or process by mathematical means. On the other hand, much useful information can be developed through systematic evaluation of sequences of idealized working models with reference to the data of

interest.

Errors associated with the choice of model are called errors of idealization whereas errors associated with finite element or other numerical approximation of the exact solution of the model are called errors of discretization. The process by which errors of idealization are controlled is called validation. The process by which errors of discretization are controlled is called verification. In this paper control of both the errors of idealization and discretization are discussed with reference to a model problem for which detailed experimental information of high quality is available.

The model problem discussed in this paper is the first of four models investigated by experimental and analytical means at Oak Ridge National Laboratory in the 1970's [15], [14]. The test articles consisted of two thin-walled circular cylindrical shells intersecting at right angles. The cylindrical shells were made of carbon steel. The test articles are idealized representations of shell intersections that occur in piping and pressure vessel systems in the sense that there were no transitions, fillets or reinforcements at the junctions. The stated objective of the experiments was to obtain stress data for comparison with the predictions of thin shell theory.

A hierarchic family of working models that allow virtually arbitrary representation of the transverse variation of the displacement vector components is described in the following. The lowest member of the hierarchy is similar to the Naghdi shell model. The highest member is the fully three-dimensional representation. Selection of a working model for a particular application is based on feedback information that includes the results of tests conducted with the objective to determine whether the data of interest are dependent on the restrictive assumptions incorporated in the model.

4.1 Experiments

Physical experiments were performed at the Oak Ridge National Laboratory in the 1970's [14], [15]. The goal of the experiments was to determine whether the classical model for shells, known as the Novozhilov-Koiter model, discretized by an assembly of flat plate elements, is capable of predicting strains in the vicinity of the intersection of two cylindrical shells. Four carbon steel test articles were manufactured and instrumented with great care. A detailed analysis of the first test article, based on hierarchic modeling techniques, is available in [18].

The first test article was made by welding two carbon steel pipes then carefully machining the weldment to the test dimensions. The test article was annealed at several points in the machining process. The experimental arrangement is shown in Fig. 8. The horizontal part is called the cylinder, the vertical part is called the nozzle. The length of the cylinder was 39.0 in (991 mm). The length of the nozzle, measured from the point of intersection of the centerline of the nozzle with the centerline of the cylinder was 19.5 in (495 mm). The outside diameter of the cylinder (resp. nozzle) was 10 in (254 mm) (resp. 5.0 in (127 mm)). The intended wall thickness of the cylinder (resp. nozzle) was 0.1 in (2.54 mm) (resp. 0.05 in (1.27 mm)).

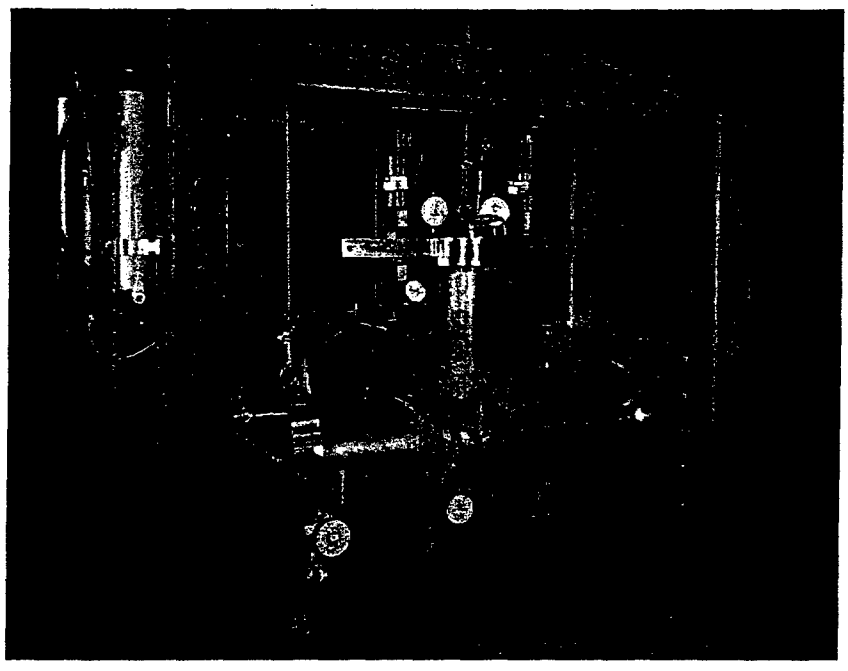

Figure 8: Experimental arrangement. Reproduced with permission from Oak Ridge National Laboratory.

4.1.1 Constraint conditions

As shown in Fig. 8, the right end of the cylinder was rigidly clamped to a heavy flat plate bolted to a frame. Small flanges were machined into the ends of the cylinder and nozzle to support the seal and the clamping forces. Heavy loading fixtures were attached on the left end of the cylinder and the end of the nozzle to provide seal and seating for the application of forces.

4.1.2 Loading conditions

A total of thirteen (13) load cases that included pressure loading and axial forces, shear forces and moments were investigated. The forces and moments were applied to the cylinder and the nozzle through hydraulic rams acting through load cells. The pressure loading was applied by means of a hydraulic fluid. In order to compensate for the weight of the hydraulic fluid, a counterbalancing force was applied to the fixture at the free end of the cylinder through a cable that is visible in Fig. 8.

For all 13 load cases the load was applied in increments of 20 percent of the full load, then decreased to zero again in 20 percent decrements. In this paper only one of the loading cases, the pressure load, is discussed. Additional load cases are discussed in [18]. The maximum value of the pressure was 50.0 psi (344.8 kPa).

4.1.3 Measurements

A total of 322 three-gauge (Micro-Measurements type EA-06-030YB-120, option SE) foil rosettes were bonded on the inside and outside surfaces by epoxy adhesive and cured. The gauges in the rosettes were arranged in a 'Y' pattern (i.e., the directions of measurement were 120 degrees apart) [14]. Details of the instrumented intersection region is shown in Fig. 9.

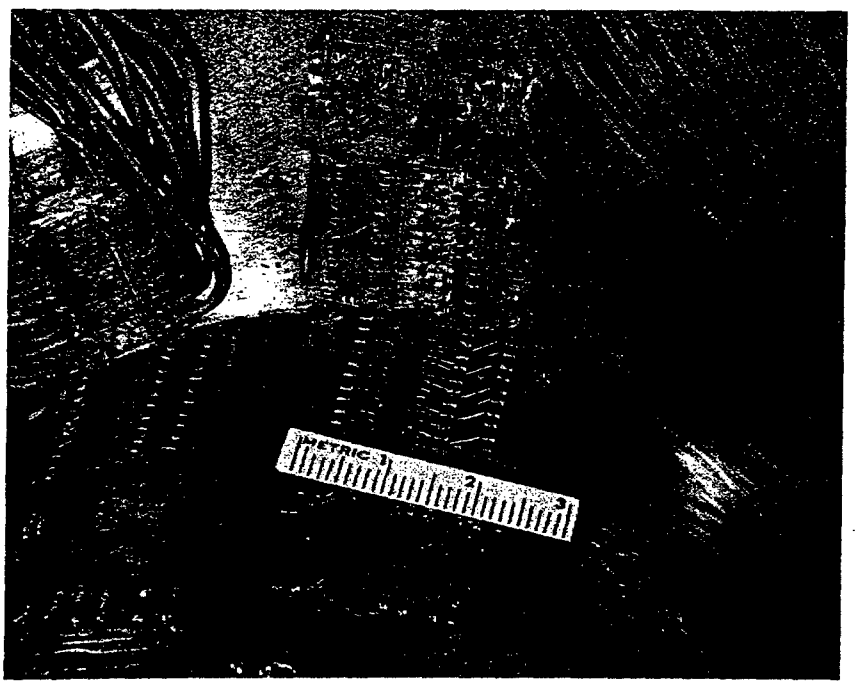

Figure 9: Detail of test article instrumented with strain gauges. Reproduced with permission from Oak Ridge National Laboratory.

The ratio of the resistance change in a strain gauge to the Lagrangian strain causing the change is called the gauge factor. The gauge factor of each production lot is determined by sample measurements and is given on each package with its tolerance. Typical tolerances are 0.5 to 1.0 %. No tolerance data are provided in references [14], [15].

4.2 Formulation

The formulation of working models for structural shells is a large and complicated subject that cannot be discussed in sufficient detail here. Only a brief overview of the main points relevant to the present investigation is presented.

4.2.1 Kinematic assumptions

A structural shell is characterized by a surface, called mid-surface x_i, and the thickness t. Both are given in terms of two parameters α_1, α_2:

$$x_i = x_i(\alpha_1, \alpha_2), \quad t = t(\alpha_1, \alpha_2).$$

The indices for α_i take on the values $i = 1, 2$ whereas the indices of x range from 1 to 3. Associated with each point of the mid-surface are three basis vectors. Two of the basis vectors lie in the tangent plane:

$$b_i^{(1)} := \frac{\partial x_i}{\partial \alpha_1}, \qquad b_i^{(2)} := \frac{\partial x_i}{\partial \alpha_2}.$$

Note that $b_i^{(1)}$ and $b_i^{(2)}$ are not necessarily orthogonal. The third basis vector $b_i^{(3)}$ is the cross product of $b_i^{(1)}$ and $b_i^{(2)}$, therefore it is normal to the tangent plane. These are called curvilinear basis vectors. The normalized curvilinear basis vectors will be denoted by $\mathbf{e}_\alpha$, $\mathbf{e}_\beta$, $\mathbf{e}_n$. The Cartesian unit basis vectors corresponding to the coordinates x_i will be denoted by $\mathbf{e}_x$, $\mathbf{e}_y$, $\mathbf{e}_z$. A vector $\mathbf{u}$, given in terms of the curvilinear basis vectors, denoted by $\mathbf{u}_{(\alpha)}$, can be transformed to Cartesian coordinates, denoted by $\mathbf{u}_{(x)}$. The transformation is

$$\mathbf{u}_{(x)} = [R]\mathbf{u}_{(\alpha)} \tag{8}$$

where the columns of the transformation matrix $[R]$ are the unit vectors $\mathbf{e}_\alpha$, $\mathbf{e}_\beta$, $\mathbf{e}_n$. The displacement vector components are given in the following form:

$$\begin{aligned} u_\alpha &:= \sum_{i=0}^{m_\alpha} u_{\alpha|i}(\alpha, \beta)\phi_i(\nu) \\ u_\beta &:= \sum_{i=0}^{m_\beta} u_{\beta|i}(\alpha, \beta)\phi_i(\nu) \\ u_n &:= \sum_{i=0}^{m_n} u_{n|i}(\alpha, \beta)\phi_i(\nu) \end{aligned} \tag{9}$$

where ν is the independent variable in the direction of the normal. The functions $u_{\alpha|i}$, $u_{\beta|i}$, $u_{n|i}$ are called field functions, the functions $\phi_i(\nu)$ are called director functions. When the material is isotropic then $\phi_i(\nu)$ are polynomials; when the shell is laminated then $\phi_i(\nu)$ are piecewise polynomials (see, for example, [22], [19]). Equation (9) represents a semi-discretization in the sense that $\phi_i(\nu)$ are fixed, hence the number of dimensions is reduced from three to two. The kinematic assumptions incorporated in a particular shell model are characterized by the indices (m_α, m_β, m_n). The lowest member of the hierarchy is the model (1, 1, 0) which, from the point of view of kinematic assumptions, is the same as the Naghdi shell model [20]. The kinematic assumptions of the Novozhilov-Koiter model [21] are more restrictive than those of the model (1, 1, 0) in that the field functions $u_{\alpha|1}$ and $u_{\beta|1}$ are constrained to be linear combinations of the first derivatives of $u_{n|0}$, i.e., there are only three independent field functions.

The classical development of shell models was strongly influenced by the limitations of the methods available for solving the resulting systems of equations. The use of curvilinear coordinates allowed the treatment of shells with simple geometric description, such as cylindrical, spherical and conical shells by classical methods, subject to the assumption that the thickness of the shell is small in relation to its other dimensions. Such limitations no longer exist. It is possible to formulate the problem in terms of either the curvilinear or the Cartesian components of the displacement vector. When the formulation is based on the curvilinear (resp. Cartesian) components of the displacement vector then we refer to the formulation as a shell (resp. thin solid) formulation.

In the following we will be concerned with the thin solid formulation only, that is, the formulation in terms of the Cartesian components of the displacement field:

$$\begin{aligned} u_x &:= \sum_{i=0}^{m} u_{x|i}(\alpha,\beta)\phi_i(\nu) \\ u_y &:= \sum_{i=0}^{m} u_{y|i}(\alpha,\beta)\phi_i(\nu) \\ u_z &:= \sum_{i=0}^{m} u_{z|i}(\alpha,\beta)\phi_i(\nu). \end{aligned} \tag{10}$$

Note that, in the case of thin solid models, the kinematic assumptions are characterized by the single index m. In other words, the transverse variation of the three displacement vector components is approximated by the same functions $\phi_i(\nu)$, $i = 0, 1, 2, \ldots m$.

Certain advantages and disadvantages are associated with formulating shell models in terms of the Cartesian, rather than the curvilinear, components of the displacement vector. The advantages are that continuity with other bodies, such as stiffeners, are easier to enforce and implementation is simpler. The disadvantages are that thin solid formulations cannot be applied to laminated shells unless each lamina is explicitly modeled or homogenized material properties are used; the number of field functions must be the same for each displacement component. For example, the (1, 1, 0) shell model has five field functions, the thin solid model characterized by $m = 1$ has six field functions.

4.2.2 Linear working models for shells

In the hierarchic view of working models the highest (i.e., most comprehensive) model accounts for all possible nonlinear effects, such as geometric nonlinearities, material nonlinearities and mechanical contact. In the case of beams, plates and shells there is an important subset of model hierarchy where the highest model is the fully three-dimensional problem of linear elasticity. For this subset, the accuracy of the exact solution of a working model is understood to be in relation to the exact solution of the corresponding fully three-dimensional problem of linear elasticity, not the underlying problem of solid mechanics. This subset is discussed in this section.

The vector of strain tensor components corresponding to $\mathbf{u}$ is denoted by $\{\epsilon\}$. The relationship between $\mathbf{u}$ and $\{\epsilon\}$ is given by $\{\epsilon\} = [D]\mathbf{u}$ where $[D]$ the differential operator associated with small strain elasticity. The vector of stress tensor components is denoted by $\{\sigma\}$. The relationship between $\{\sigma\}$ and $\{\epsilon\}$ is given by Hooke's law: $\{\sigma\} = [E]\{\epsilon\}$ where $[E]$ is the elastic material stiffness matrix. Traction vectors acting on $\partial\Omega$ are denoted by $\mathbf{T}$. The virtual work of internal stresses is defined as follows:

$$B(\mathbf{u},\mathbf{v}) := \int_\Omega ([D]\mathbf{v})^T[E][D]\mathbf{u}\, d\Omega \tag{11}$$

and the virtual work of external forces is defined by

$$F(\mathbf{v}) := \int_\Omega \mathbf{F}\cdot\mathbf{v}\, d\Omega + \int_{\partial\Omega} \mathbf{T}\cdot\mathbf{v}\, dS + \int_\Omega ([D]\mathbf{v})^T[E]\{c\}\tau\, d\Omega \tag{12}$$

where $\{c_t\} := \{c_t\ c_t\ c_t\ 0\ 0\ 0\}^T$, c_t is the coefficient of thermal expansion and $\tau = \tau(x,y,z)$ is the change in temperature from a reference temperature.

The energy space is defined by $E(\Omega) := \{\mathbf{u}\,|\,B(\mathbf{u},\mathbf{u}) \le C < \infty\}$ where C is some positive constant. The energy norm is defined by

$$\|\mathbf{u}\|_{E(\Omega)} := \left(\frac{1}{2}B(\mathbf{u},\mathbf{u})\right)^{1/2}. \tag{13}$$

The generic form of the principle of virtual work is stated as follows: Find $\mathbf{u} \in E(\Omega)$ such that

$$B(\mathbf{u},\mathbf{v}) = F(\mathbf{v}) \qquad \text{for all } \mathbf{v} \in E(\Omega). \tag{14}$$

Specific statements of the principle of virtual work depend on the boundary conditions. For details we refer to [7]. In the generic case, and whenever the prescribed displacement constraints are insufficient to prevent all possible rigid body displacements, the solution of eq. (14) is unique up to rigid body displacements.

There is an important difference between the classical shell models, such as the Novozhilov-Koiter and the Naghdi model, and the hierarchic shell and thin solid models. In using hierarchic models the goal is to approximate the fully three-dimensional solution, hence the stress-strain law is that of the three-dimensional theory of elasticity. In index notation:

$$\sigma_{ij} = \lambda\delta_{ij}\epsilon_{kk} + 2\mu\epsilon_{ij} \tag{15}$$

where σ_{ij}, ϵ_{ij} are the Cartesian stress and strain tensors, respectively, λ and μ are the Lamè parameters and δ_{ij} is the Kronecker delta. Incorporated in the stress-strain relationship of the Naghdi and the Novozhilov-Koiter models is the assumption that the stress component normal to the mid-surface is zero, a condition which is the limiting case of the fully three-dimensional solution with respect the thickness approaching zero. The Naghdi shell model yields the correct solution in the limit $t \to 0$, however neither the hierarchic shell model (1, 1, 0) nor the thin solid model $m = 1$ does, unless Poisson's ratio is zero. The Naghdi model is not a member of the hierarchic sequence of models but rather an extension of the sequence for small t values. Hierarchic shell (resp. thin solid) models characterized by $m_n \ge 3$ (resp.

$m \geq 3$) give the correct limit solution with respect to $t \to 0$ and are said to be asymptotically consistent.

Remark 4.1 In the case of shells the distinction between the notions of mathematical model and its discretization is blurred by conventions in terminology: It is customary to refer to the various shell formulations as theories or models. In fact, the hierarchic models are semi-discretizations of the fully three-dimensional model. Therefore modeling errors that can be attributed to the choice of indices (m_α, m_β, m_n) in the case of hierarchic shell models, and the index m in the case of thin solid models, are related to discretization rather than model definition.

4.2.3 Nonlinear working models for shells

The model hierarchy must account for nonlinear effects. This large and important topic is not within the scope of this paper. For discussion and examples we refer to [16], [17], [23].

4.3 Finite element spaces

The accuracy of the finite element solution is determined by the finite element space. Finite element spaces are constructed by partitioning the solution domain Ω into finite elements. A partition will be denoted by Δ, the number of elements of the partition by $M(\Delta)$ and the kth element by Ω_k. Typically Ω_k is mapped from a corresponding standard element Ω_{st} by smooth mapping functions $\mathbf{Q}^{(k)}$.

Ideally, finite element spaces are constructed by adaptive methods such that the tolerance criteria for the data of interest are satisfied. The initial finite element mesh should be laid out utilizing a priori information concerning the regularity of the exact solution. For example, in the neighborhood of singular points and lines the mesh should be graded in geometric progression with a fixed common factor when p-extension is used [7]. If h-extension is used then radical grading is optimal [24]. In the case of plate and shell models the presence of boundary layers has to be taken into account.

4.3.1 The finite element space used in the ORNL investigation

At the time of the ORNL investigation the treatment of shell models by the finite element method was in its very early stages of development. Although the investigators were aware of some contemporary work on curved shell elements, shells were commonly approximated by flat plate elements and most of the available experience was with those elements. For this reason the investigators decided to use flat plate elements for the purpose of analyzing the shell intersection problem [14]. The Hsieh-Clough-Tocher (HCT) triangular element [25] was chosen for the approximation of the displacement component normal to the mid-surface of the shell. The constrained linear strain triangle (CLST) was used for approximating the membrane components. A brief description follows.

The HCT triangle is a composite element, comprised of three sub-triangles. On each sub-triangle an incomplete cubic polynomial approximation, comprised of 9 terms, is used. The polynomials are chosen so that along the external edges the normal derivative varies linearly. Therefore there are 9 coefficients per sub-triangle. C^0 continuity is enforced for the sub-elements by constructing basis functions corresponding to the 3 nodal displacements and 6 rotations for each sub-triangle, as indicated in Fig. 10(a) where the circles represent transverse displacements and the arrows represent first derivatives (rotations in the sense of the arrows). The sub-triangles are assembled, which is equivalent to satisfying C^0 continuity over the triangle.

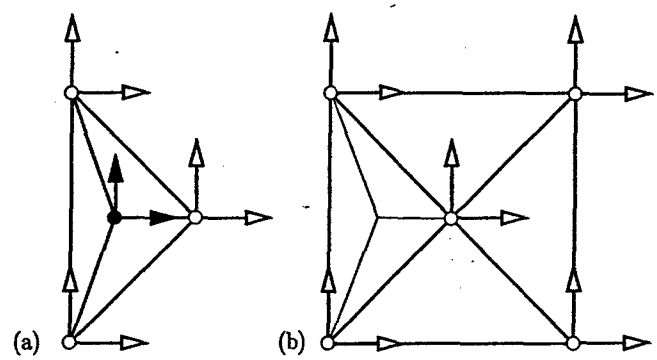

Figure 10: (a) The 12 degrees of freedom HCT triangle. (b) Composite non-planar quadrilateral element assembled from four HCT triangles.

At this point there are 3 internal degrees of freedom, indicated in Fig. 10(a) by the closed circles and arrows, and 9 external degrees of freedom, indicated by the open circles and arrows. In order to satisfy exact and minimal C^1 continuity, the continuity of the normal derivatives along the internal edges is enforced leading to 3 constraint equations that establish a relationship between the sets of internal and external degrees of freedom. Using these constraint equations the internal degrees of freedom are eliminated. Thus the HCT triangle has 9 degrees of freedom: three displacements and three rotations in each coordinate direction.

Non-planar quadrilateral plate elements assembled from four HCT elements were used for approximating the displacement vector components normal to the shell surface. A typical element is shown in Fig. 10(b). Since the center node generally does not lie in the same plane as the vertex nodes, there is a third rotation component, not present in the constituent triangles. A third rotation component is also present in the assembly of the quadrilateral elements into the stiffness matrix, since adjacent elements are generally not co-planar. The usual treatment is that the rotation components are transformed into a Cartesian system, the origin of which lies on the shell surface at the node and one axis is coincident with the normal to the surface. The rotation component in the direction of the normal is usually neglected. This causes various problems, for details we refer to [14], [15], [26]. For a discussion on low order shell elements we refer to [12].

The in-plane (membrane) components of the displacement vector were approximated by a similar assembly of triangles. These vector components were approximated over each

component triangle by quadratic polynomials constrained so that the variation is linear over the external edges. This is known as the constrained linear strain triangle (CLST). A quadrilateral membrane element has two degrees of freedom at each of its five nodes [14]. The finite element space is the span of the assembled of HCT and CLST triangles shown in Fig. 11.

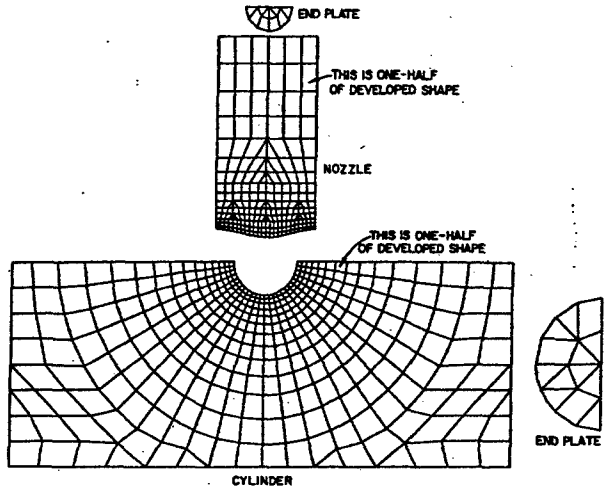

Figure 11: Finite element mesh used in the ORNL investigation. There are 649 nodal points of which 25 nodal points lie on the intersection. Source: ORNL-DWG 69-10664R. Reprinted with permission from Oak Ridge National Laboratory.

The investigators recognized two sources of error: The errors caused by using plate elements rather than curved shell elements and by using a limited number of elements. Implied is the tacit assumption that, as the number of elements is increased, the approximate solution will converge to the exact solution of the Novozhilov-Koiter shell model. This has not been proven. There is no guarantee that the sequence of finite element solutions obtained by h-extension will converge to the exact solution of the Novozhilov-Koiter model of this problem.

Remark 4.2 The definition of the HCT triangle given in [13] is different from the one described here in that all sub-triangles are complete polynomials of degree 3 in which case there are 12 degrees of freedom, the nine degrees of freedom shown in Fig. 10(a) plus the first derivative in the direction of the normal at the mid-point of each side.

4.3.2 The finite element spaces used in the present investigation

In the present investigation the thin solid formulation implemented in the finite element analysis software product StressCheck[5]. was used. The finite element mesh, consisting of 188 elements, is shown in Fig. 12. The nozzle and the shell were partitioned into hexahedral

[5]StressCheck is a trademark of Engineering Software Research and Development, Inc., St. Louis, Missouri.

elements, the intersection region was partitioned into hexahedral and pentahedral elements. The hexahedral elements were mapped from the standard hexahedron

$$\Omega_{\rm st}^{(h)} := \{(\xi,\eta,\zeta)\,|\,|\xi|<1,\ |\eta|<1,\ |\zeta|<1\} \tag{16}$$

by smooth mapping functions. For details on mapping procedures we refer to [27].

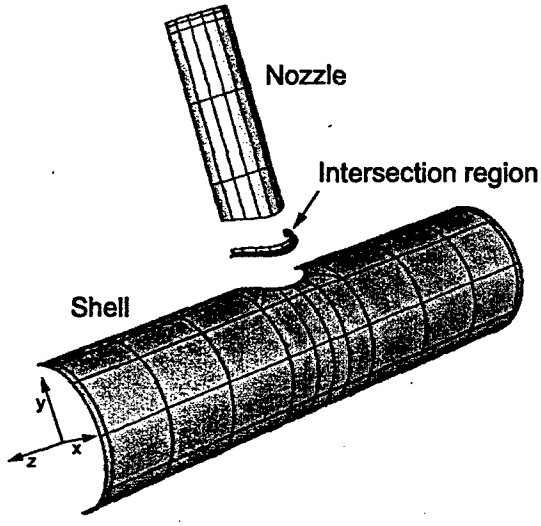

Figure 12: The 188-element mesh used in the present investigation.

The standard polynomial spaces used in the present investigation are known as anisotropic trunk spaces. For $p>1$, $1\le q\le p$ these spaces are defined by:

$$\begin{aligned} S_{\rm tr}^{ppq}(\Omega_{\rm st}^{(h)}) := \text{span}(&\xi^k\eta^\ell\zeta^m, \xi^p\eta\zeta^m,\ \xi\eta^p\zeta^m,\ (\xi,\eta,\zeta)\in\Omega_{\rm st}^{(h)},\\ &k,\ell=0,1,2,\ldots,\ k+\ell\le p,\ m=0,1,2\ldots,q). \end{aligned} \tag{17}$$

For definitions of the isotropic trunk space on the standard hexahedron $S_{\rm tr}^{p}(\Omega_{\rm st}^{(h)})$, and the standard pentahedron $S_{\rm tr}^{p}(\Omega_{\rm st}^{(p)})$ we refer to [7]. The finite element space $S(\Omega)$ is the span of the mapped basis functions defined on the standard elements, subject to the exact and minimal continuity requirement of the formulation. Referring to eq. (10), $q=m$, corresponds to the thin solid formulation characterized by the index m. For additional details we refer to [16], [23], [28].

4.4 Working models

The quality of a working model is determined by the proximity of its exact solution to the exact solution of the state of the art model, more precisely, the proximity of functionals that would be computed from the exact solution of the state of the art model and the working model. Here we examine a sequence of working models from the point of view of their ability to approximate physical observations and data computed from physical observations through simple transformation.

The objective of the ORNL experiments was to investigate how well thin shell theory is capable of predicting the stress distribution in intersecting cylindrical shells in the neighborhood of the intersection. The investigators had in mind the Novozhilov-Koiter shell model only. This model is a reasonable choice for representing the smooth parts of the intersecting shells. However, given that the data of interest are the strain values in the vicinity of the intersection, neither the kinematic assumptions nor the material properties (plane stress) incorporated in this model are valid in that region. Whereas the mathematical problem of the intersecting cylinders for the Novozhilov-Koiter shell model is well defined [29], it is not a good representation of the physical problem.

The working models employed in the present investigation were also based on the theory of elasticity but differ from the Novozhilov-Koiter shell model in kinematic assumptions and material properties, as described in Section 4.2. The intersection region was treated as a three-dimensional elastic region for each model. The size of the intersection region (characterized by the dimensions d_s and d_n shown in Fig. 13) is fixed for each working model. Elsewhere the kinematic assumptions of the thin solid formulation were used with $m = q = 1, 2, \ldots$

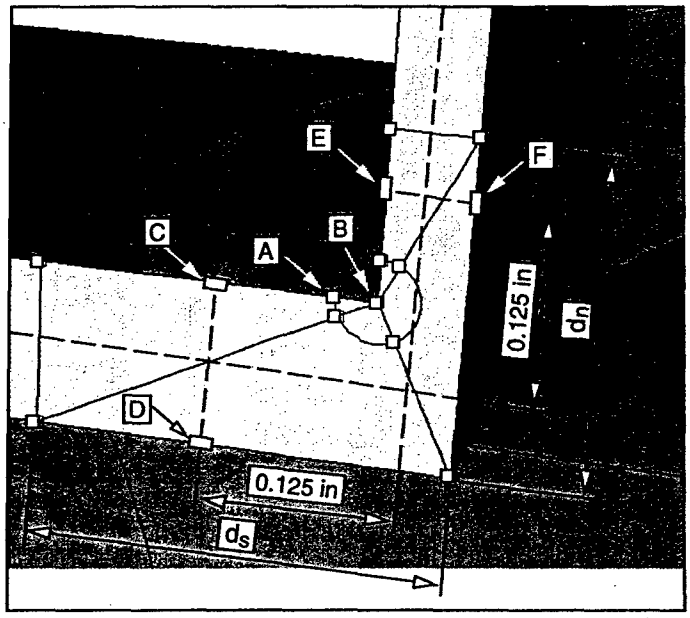

Figure 13: Mesh detail at the intersection region and location of the strain gauges in the plane of symmetry nearest to the intersection. 188-element mesh.

The problem of selecting a working model with respect to the goals of computation of the ORNL experiments is understood as follows: A particular working model based on the thin solid formulation is judged to meet the necessary conditions for acceptance if the equivalent (von Mises) stresses computed in the gauge locations do not differ by more than τ percent from the corresponding equivalent stresses computed from the fully three-dimensional model. The choice of tolerance is, of course, arbitrary, however the accuracy required of the numerical solution depends on this choice. The relative error in the numerical solution has to be less

than approximately 0.5τ percent.

Using the 188-element mesh shown in Fig. 12 and the anisotropic spaces $S_{\rm tr}^{ppq}(\Omega_{\rm st}^{(h)})$ with $q = 1, 2, \ldots, 8$ all working models yielded consistent results within the prescribed tolerance of $\tau = 2.5$ %. Therefore the simplest model ($q = 1$) is preferred.

In comparing data computed from working models with physical measurements, it is necessary to recognize the differences between the mathematical problem being solved and the physical system being modeled. These differences are enumerated in relation to the ORNL test article in the following.

1. Geometric variations. The ORNL investigators were careful to minimize errors in manufacturing the test article however, owing to unavoidable machining tolerances, some variations in wall thickness and the other dimensions had to be present. Quoting from reference [14];

   > *"A careful dimensional inspection of the machined model indicated that, despite the care taken in machining, there were wall thickness variations in both nozzle and cylinder with the nozzle thickness being as much as* 15 % *greater (0.007 to 0.008 in. compared with the nominal 0.050 in) in the fourth quadrant than in the second."*

   In the working models it is assumed that the shells are defined by perfect cylindrical surfaces and constant wall thickness.

   The intent of the ORNL investigators was to manufacture the intersection with zero fillet radius. In reality, the milling tool leaves some fillet, see Fig. 9. In the working models the fillet radius is zero.

   The test article had small flanges at the ends. The working models do not account for those flanges.

2. Variations in material properties. The material properties assumed by the ORNL investigators are the nominal elastic constants of carbon steel. Modulus of elasticity: $E = 30 \times 10^6$ psi (207 GPa); Poisson's ratio: $\nu = 0.3$. The actual elastic constants of the test article can differ from the nominal values by a few percent. There are no data on the statistical variations of the modulus of elasticity and Poisson's ratio, however it is reasonable to expect that the mean value of E (resp. ν) is within about 2 % (resp. 5 %) of the nominal value. Therefore systematic as well as random errors are present in making comparisons between measured strains and strains computed from the working models.

   The relationship between stress and strain in the test article will become nonlinear when the strain corresponding to the proportional limit is exceeded. In the working models examined herein the material is assumed to be perfectly elastic, independently of the magnitude of strain.

3. Differences in constraint conditions. Rigid end fixtures were attached to the free end of the cylinder and the nozzle, as described in Section 4.1.1. Details on the end fixtures

are not given in the ORNL reports, however the investigators assumed that the end fixtures were sufficiently rigid to constrain the ends of the cylinder and nozzle so as to maintain the ends as plane circles [14]. In the working model constructed by the ORNL investigators the end fixtures were represented by end plates. In the present investigation the fixture attached to the nozzle was represented by an end plate. At the free end of the cylinder the radial and tangential displacement components were set to zero.

4. Differences in loading conditions. The test article was loaded through hydraulic rams acting on the end fixtures. The accuracy of the applied load, and hence the accuracy of the stress resultants, was determined by the accuracy of the load cells. The transfer of the load through the end fixtures was through mechanical contact. The precise distribution of the tractions acting on the ends is not known. In the working models used in the present investigation uniform tractions were applied on the free end of the cylinder.

5. Symmetry. The working model was assumed to be perfectly symmetric. The test article was not perfectly symmetric and, very likely, the strain gauges were not installed to be perfectly symmetric.

It is seen that even under very carefully controlled experimental conditions some degree of uncertainty concerning the physical system is present. Some of these uncertainties can be reduced, other uncertainties either cannot be reduced or may not be feasible to reduce. For example, the mean value of the elastic constants can be determined by simple coupon tests. The dimensions of the test article can be measured with high accuracy. On the other hand, it would be very difficult to determine the distribution of the tractions or constraint conditions imposed by the end fixtures. In addition, some degree of uncertainty is associated with the instruments employed in making the observations and the effects of the environment on the instruments.

In view of these uncertainties one cannot expect very close correlation between computed and experimental data. In the ORNL experiments the largest uncertainties are caused by the difficulties associated with manufacturing thin-walled objects to tight tolerances and mathematical representation of the constraint conditions.

4.5 Numerical results

It is necessary to ascertain that the errors in the computed data are well below the threshold set for rejection of a working model. In this investigation the following steps were taken: (a) The relative error in energy norm was estimated. This provides an overall view of the quality of the approximation. The error in energy norm is roughly equivalent to the RMS error in stresses [7]. For the 188-element mesh the estimated relative error in energy norm ranged between 1.15 and 3.20 percent. (b) The dependence of the data of interest on the mesh and the polynomial degree of elements was examined. It was found that the data of interest are substantially independent of the mesh and the polynomial degree of elements.

(c) The data of interest were examined for jump discontinuities at inter-element boundaries. Substantial jump discontinuities in locations where the data should be continuous is an indication that the discretization is inadequate. No significant discontinuities were found. These are necessary conditions that an approximate solution will satisfy when the errors of approximation are not large.

Due to space limitations, only some of these procedures are illustrated in the following. Details of the finite element mesh in the shell intersection region are shown in Fig. 13. The size of the shell intersection region is characterized by the dimensions d_s and d_n. Unless otherwise stated, in the numerical investigation described herein these dimensions were fixed: $d_s = 0.25$ in (6.35 mm); $d_n = 0.20$ in (5.08 mm).

The layout of the mesh in the intersection region is typical of meshes used in p-extensions when corner singularities are present [7]. Nodal point B lies on the line of intersection between the outer surface of the nozzle and the outer surface of the shell in the plane of symmetry. Nodal point A lies on the line of intersection between the outer surface of the shell and the plane of symmetry.

The convergence of the equivalent stress at Point A, with respect to the number of degrees of freedom N, is shown in Fig. 14 on a semi-log scale for the fully three-dimensional model. It is seen that the stress is substantially independent of the polynomial degree p for $p \geq 5$. The equivalent stress computed from the finite element solution cannot be close to its exact value if this criterion is not satisfied.

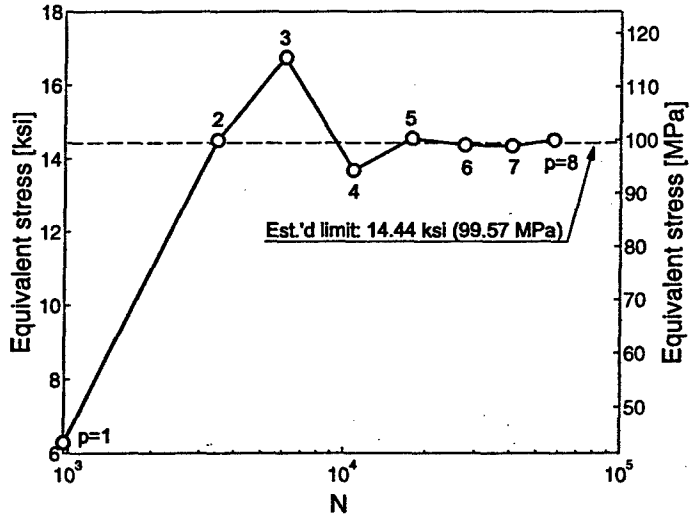

Figure 14: Convergence of the equivalent stress at Node A shown in Fig. 13. 188-element mesh.

A similar plot shown in Fig. 15 for the equivalent stress computed for point B clearly indicates divergence. This is caused by the presence of an edge singularity. The equivalent stress computed for the exact solution of the elasticity problem is infinity in this point, hence the equivalent stress computed from the finite element solution cannot converge to a finite value. Consequently, extrapolation of strain data from the gauge locations to the intersection is not permissible.

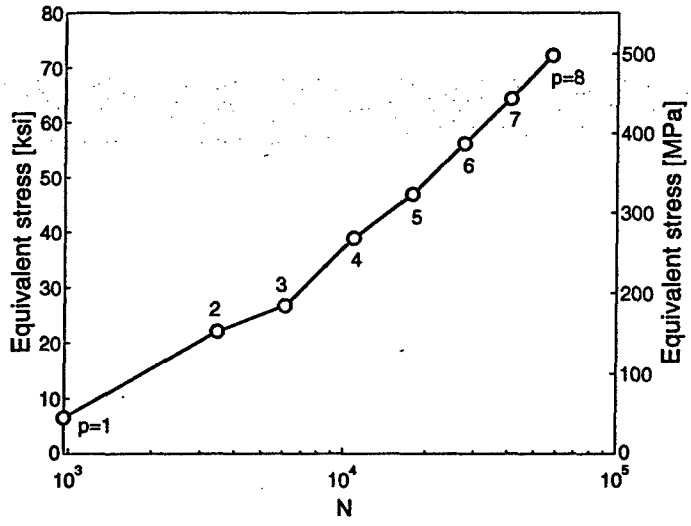

Figure 15: Convergence of the equivalent stress at Node B shown in Fig. 13. 188-element mesh.

Equivalent stresses in strain gauge locations nearest to the intersection region in the plane of symmetry (toward the fixed-end of the cylinder) are shown in Table 1. These data were computed from the solutions obtained for the fully three-dimensional model with p ranging from 1 to 8. The number of degrees of freedom (N) are shown in the second column. Points C, D, E and F are shown in Fig. 13. Each stress value converges strongly to a limit value, similar to the convergence shown in Fig. 14. The corresponding experimental data and the relative differences (DIFF), using the computed values as the base, are shown in the last two rows. It is seen that the differences are very substantial in three of the four points.

Table 1: EQUIVALENT STRESSES (PSI) IN THE GAUGE LOCATIONS C, D, E, F IDENTIFIED IN Fig. 13. FULLY THREE-DIMENSIONAL MODEL. THE POINTS ARE LOCATED ON THE FIXED-END SIDE OF THE CYLINDER (1 PSI=6.895 kPa).

p	N	Pt. C	Pt. D	Pt. E	Pt. F
3	6095	11225	11959	13729	16589
4	10828	12461	11680	16729	19687
5	17774	12455	12158	17644	19441
6	27497	12535	12089	17237	19005
7	40561	12542	12021	17108	19104
8	57530	12544	11982	17094	18903
EXPT		15569	14554	16981	13100
DIFF. (%)		28.6	24.1	-0.3	-28.9

These differences are attributed primarily to variations in wall thickness. All other uncertainties would have a much smaller effect. Inspection of the test article revealed variations in wall thickness as large as 15 % [14]. Variations in wall thickness affect both the distribution and magnitude of stresses. The magnitude of these effects depends on whether the solution

is bending- or membrane-dominated. Assuming that the bending moments and membrane forces are independent of the wall thickness, in a bending (resp. membrane) dominated region 10% change in wall thickness causes approximately 24% (resp. 11%) change in stress.

In experiments designed for purposes of validation it is necessary to eliminate uncertainties with respect to the object of the experiment as much as possible [30]. In the ORNL test article described in this paper the dominant source of uncertainty is the unknown variation in wall thickness. Ideally, the external and internal surfaces would be carefully measured and the actual surfaces would be used in the working model. With today's technology it would be possible to produce a CAD model of the test article as manufactured, to within 0.001 in (0.025 mm) tolerance. The complexity of the resulting geometrical description of the test article would make construction of the working model significantly more complicated, however.

In the immediate vicinity of the junction there are large bending moments that decay with respect to distance from the junction. The computed and experimentally obtained values of the equivalent stress in gauge locations along the line of intersection of the plane of symmetry with the outer surface of the cylinder on the fixed end side are tabulated in Table 2. It is seen that the errors are larger near the junction than away from it, and the errors are roughly consistent with approximately 10% variation in wall thickness. The magnitude of the actual variation is unknown.

Table 2: COMPUTED (FEA) AND EXPERIMENTALLY (EXP) OBTAINED VALUES OF THE EQUIVALENT STRESS (PSI) IN GAUGE LOCATIONS ON THE INTERSECTION OF THE PLANE OF SYMMETRY WITH THE OUTSIDE SURFACE OF THE CYLINDER AS A FUNCTION OF THE DISTANCE (s) FROM THE MID-SURFACE OF THE NOZZLE (INCHES).

s	FEA	EXP	err (%)
0.125	12541	15569	24.14
0.250	10129	12381	22.23
0.375	8190	8870	8.31
0.500	6531	7453	14.13
0.625	5086	5783	13.70
1.000	2105	2242	6.49
1.500	1836	1844	0.42
2.000	2343	2230	-4.84
3.000	2431	2292	-5.71

The other sources of error are inelastic deformation in the vicinity of the junction, variations in material properties, errors in the location of the strain rosettes, errors in measurement, errors caused by idealization of the actual constraint condition and errors in loading. None of these errors are large enough to explain the observed differences. For example, to test the effect of inelastic deformation, elastic perfectly plastic material behavior was assumed, the yield stress being 36.0 ksi (248 MPa). Using the deformation theory of plasticity it was found that the plastic zone was confined to a very small neighborhood of the line of intersection of the outer surfaces and hence its effect on the stresses in the gauge locations

was negligible. For a discussion on the other effects we refer to [18].

A comparison between data computed from experimental measurements and data computed from the fully three-dimensional working model along the inner surface of the cylinder, measured from the mid-surface of the nozzle, is shown in Fig. 16.

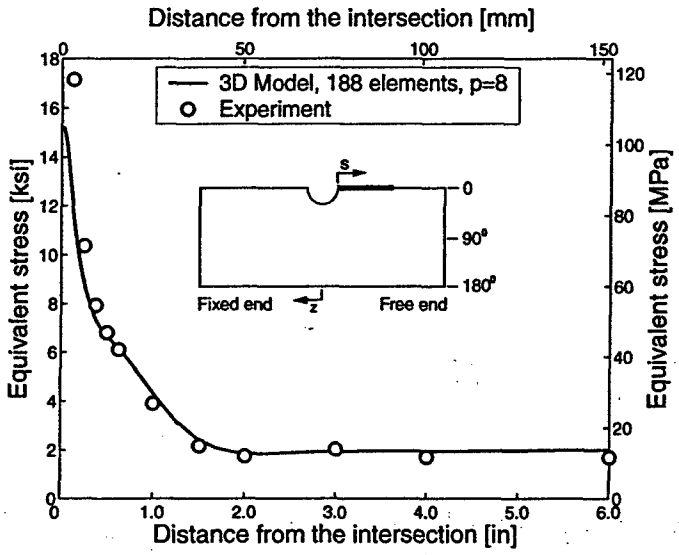

Figure 16: Equivalent stress on the inside surface of the cylinder vs. distance from the mid-surface of the nozzle.

Equivalent stresses computed in the strain gauge locations labelled C, D, E, F in Fig. 13 (see also Table 1) from solutions obtained by means of the hierarchic thin solid models based on the spaces $S_{\rm tr}^{ppq}(\Omega_{\rm st}^{(h)})$ are shown in Table 3. The estimated relative errors in energy norm, denoted by $(e_r)_E$, are also given in Table 3. These estimates are based on p-extension. Details are available in [7]. It is seen that the stress data are insensitive to the choice of thin solid model characterized by q.

Table 3: EQUIVALENT STRESSES (PSI) IN THE GAUGE LOCATIONS C, D, E, F IDENTIFIED IN Fig. 13. THIN SOLID MODELS. THE POINTS ARE LOCATED ON THE FIXED-END SIDE OF THE CYLINDER (1 PSI=6.895 kPa).

$d_s = 0.25$ in (6.35 mm), $d_n = 0.2$ in (5.08 mm)							
p	q	$(e_r)_E$	N	Pt. C	Pt. D	Pt. E	Pt. F
8	1	3.20	41032	12110	11730	16926	18432
8	2	1.15	44766	12570	11978	17094	18904
8	3	1.35	47832	12552	11979	17094	18904
8	8	1.35	57530	12544	11982	17094	18903

One of the modeling assumptions is the selection of the size of the intersection region indicated in Fig. 13 by labels d_s and d_n. The data presented so far was computed with

Table 4: EQUIVALENT STRESSES (PSI) IN THE GAUGE LOCATIONS C, D, E, F IDENTIFIED IN Fig. 13. THIN SOLID MODELS. THE POINTS ARE LOCATED ON THE FIXED-END SIDE OF THE CYLINDER (1 PSI=6.895 kPa).

$d_s = 0.13$ in (3.30 mm), $d_n = 0.15$ in (3.81 mm)							
p	q	$(e_r)_E$	N	Pt. C	Pt. D	Pt. E	Pt. F
8	1	2.44	41032	12111	12470	17076	18169
8	2	1.11	44766	12621	12026	17104	19141
8	3	1.32	47832	12564	11941	17104	19143
8	8	1.31	57530	12546	11964	17106	19143

$d_s = 0.25$ in (6.35 mm) $d_n = 0.20$ in (5.08 mm). Therefore points C, D, E, F were located within the intersection region. Letting $d_s = 0.13$ in (3.30 mm) $d_n = 0.15$ in (3.81 mm) the points are located in the thin solid region. Repeating the computations the results shown in Table 4 are obtained. On comparing Table 3 with Table 4 it is seen that the differences are negligibly small. This indicates that the working models are insensitive to the size of the intersection region.

4.6 Summary and conclusions

The intent of the ORNL investigation was to determine whether the finite element space characterized by the mesh shown in Fig. 11 and the HCT plate elements, combined with the CLST plane stress elements, are capable of approximating strains in the given gauge locations. We understand this problem to consist of three parts: (a) Whether the Novozhilov-Koiter model is capable of representing the deformation of the test article in the intersection region; (b) whether the three-dimensional assembly of planar plate and membrane elements converge to the exact solution of the Novozhilov-Koiter model as the size of the elements is reduced, and (c) whether the mesh shown in Fig. 11 is suitable for controlling the errors of discretization. The ORNL investigation did not address these questions separately.

In the present investigation the need to address these questions was avoided by (a) demonstrating that hierarchic thin solid formulations provide consistent results in the gauge locations even for the lowest member of the hierarchy, characterized by $q = 1$; (b) curved elements mapped by smooth functions rather than planar elements were used, and (c) the data of interest were shown to be substantially independent of the discretization. Another important difference between the present investigation and the ORNL investigation is that in the present investigation the intersection region was exempt from the kinematic assumptions of the thin solid formulation.

The ORNL investigation highlights some of the difficulties and limitations of experimental validation of working models for shell problems. The experimental data are dominated by uncertainties caused by difficulties associated with the fabrication of thin-walled objects to exacting tolerances. Increasing the wall thickness would reduce errors caused by manufacturing tolerances but then the thin shell model may not be applicable.

The primary objective in defining a working model is to account for all physical laws and relationships that have a significant influence on the data of interest. Therefore the choice of a working model depends on the data of interest and has to be validated with respect to the data of interest. The secondary objective is to identify the simplest working model that will satisfy the tolerances set for the data of interest.

In correlation with experimental observations a working model is tested against data that are either observable or can be computed from observable data. In the model problem discussed herein the strain components in surface points located in the vicinity of the shell intersection were measured and the von Mises stresses were computed in the gauge locations.

The data of interest are generally not observable and cannot be computed from observable data. For example, one may be interested in the maximum value of the integral of the normal stress over some small area. Therefore, even if a working model were shown to be successful in predicting certain measured data, it may not be suitable for computing other data of interest. It is necessary to have means for systematic evaluation of the effects of various assumptions, incorporated in a working model, on the data of interest. Virtual experimentation based on a hierarchic framework of models and hierarchic discretizations is indispensable in the development of expert knowledge.

The validity of a working model cannot be established by experimental correlation in general. The purpose of validation experiments is to determine whether certain necessary conditions are met by a working model. Validation experiments cannot establish sufficient conditions for acceptance of a working model.

5 Generalized plane strain

Dimensional reduction is frequently used in engineering practice. The goal is to construct a simplified mathematical model, called *working model*, so that the exact values of the data of interest corresponding to the simplified model are substantially the same as those corresponding to the fully three-dimensional model it is expected to represent. We consider a prismatic body of length ℓ. The material points occupy the domain Ω_ℓ, defined as follows:

$$\Omega_\ell = \{(x,y,z) \,|\, (x,y) \in \omega,\ -\ell/2 < z < \ell/2,\ \ell > 0\} \tag{18}$$

where $\omega \in \mathbb{R}^2$ is a bounded domain with Lipschitz boundary. The lateral boundary of the body is denoted by

$$\Gamma_\ell = \{(x,y,z) \,|\, (x,y) \in \partial\omega,\ -\ell/2 < z < \ell/2,\ \ell > 0\} \tag{19}$$

and the faces are denoted by

$$\gamma_\pm = \{(x,y,z) \,|\, (x,y) \in \omega,\ z = \pm\ell/2\}. \tag{20}$$

The notation is shown in Fig. 17. The diameter of ω will be denoted by d_ω.

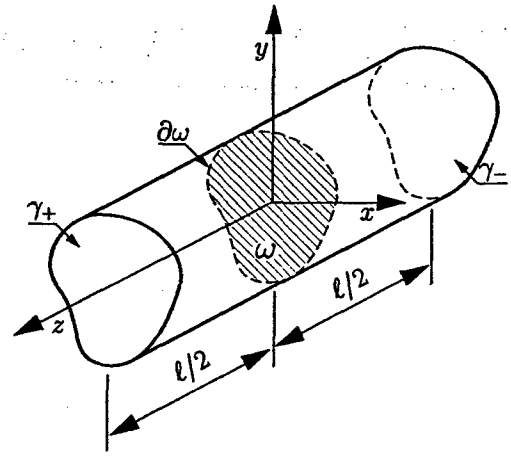

Figure 17: Notation.

The material properties, the volume forces and temperature change acting on Ω_ℓ and tractions acting on Γ_ℓ will be assumed to be independent of z. Therefore the xy plane is a plane of symmetry. It is assumed that tractions are specified on the entire boundary Γ_ℓ. This is usually called the first fundamental boundary value problem of elasticity.

When the tractions acting on $\gamma_\pm$ are zero and $\ell/d_\omega << 1$ then such problems are usually formulated on ω as plane stress problems. When the normal displacements and shearing tractions acting on $\gamma_\pm$ are zero then such problems are formulated on ω as plane strain problems, independently of the ℓ/d_ω ratio. When $1 << \ell/d_\omega$ and the tractions acting on $\gamma_\pm$ are zero then the three-dimensional thermoelasticity problem on Ω_ℓ is called the generalized plane strain problem.

The following questions were addressed: (a) Under what conditions is the plane strain solution asymptotically correct; (b) what corrections to the plane strain solution, that can be determined by solving two-dimensional problems, are necessary to obtain an asymptotically correct solution to the generalized plane strain problem, and (c) under what conditions is the plane stress solution equivalent to the generalized plane strain solution.

The conditions under which the generalized plane strain problem is asymptotically (i.e., with respect to $\ell/d_\omega \to \infty$) the plane strain solution were stated in the form of theorems. It was shown also that in special cases the generalized plane strain solution is the plane stress solution. Details and examples are available in [31].

References

[1] Uninhabited Air Vehicles: Enabling Science for Military Systems. Committee on Materials, Structures, and Aeronautics for Advanced Uninhabited Air Vehicles. National Academy of Sciences. Publication NMAB-495. National Academy Press, Washington, DC 2000.

[2] Kenendy BR. Historical Realities of the C-17 Program Pose Challenge for Future Acquisitions. *Program Manager Magazine* November-December 1999, 70–78.

[3] American Institute of Aeronautics and Astronautics (AIAA). Guide for the Verification and Validation of Computational Fluid Dynamics Simulations. AIAA-G-077-1998. Reston VA (1998).

[4] Oberkampf WL. What are validation Experiments? *Experimental Techniques* May/June 2001 35–40.

[5] Roache PJ. Verification of Codes and Calculations. *AIAA Journal* **36** (1998) 696–702.

[6] Roache PJ. *Verification and Validation in Computational Science and Engineering* Hermosa Publishers, Albuquerque, New Mexico, 1998.

[7] Szabó B and Babuška I. *Finite Element Analysis*, John Wiley & Sons, New York, 1991.

[8] Nervi S. A mathematical model for the estimation of the effects of residual stresses in aluminum plates. D.Sc. Thesis, Washington University, May 2005.

[9] Young, K. Macining-induced residual stress and distortion of thin parts. D.Sc. Thesis, Washington University, May 2005.

[10] O. C. Zienkiewicz, The Finite Element Method, 3rd ed. McGraw-Hill Book Co. London, 1977.

[11] R. D. Cook Concepts and Applications of Finite Element Analysis, 2nd Edition, John Wiley & Sons, New York, 1981.

[12] J. Pitkäränta, Mathematical and Historical Reflections on the Lowest Order Finite Element Models for Thin Structures, Computers and Structures, 81 (2003) 895-121.

[13] P. G. Ciarlet, The Finite Element Method for Elliptic Problems, North-Holland, Amsterdam (1978).

[14] Corum JM, Bolt SE Greenstreet WL and Gwaltney RC. Theoretical and Experimental Stress Analysis of ORNL Thin-Shell Cylinder-to-Cylinder Model No. 1. Oak Ridge National Laboratory Report ORNL 4553, Oak Ridge, Tennessee, October 1972.

[15] Gwaltney RC, Corum JM, Bolt SE and Bryson JW. Experimental Stress Analysis of Cylinder-to-Cylinder Shell Models and Comparisons with Theoretical Predictions. Journal of Pressure Vessel Technology, November (1976) 283–289.

[16] Rank E, Düster A, Nübel V, Preusch K, and Bruhns OT. High order finite elements for shells. *Comput. Methods Appl. Mech. Engng. (In press)*, 2005.

[17] Szabó B and Actis R. On the importance and uses of feedback information in FEA. *Applied Numerical Mathematics*, 52:219–234, 2005.

[18] Muntges D. *Validation of working models for thin cylindrical shells.* MS thesis. Washington University, The Henry Edwin Sever Graduate School, St. Louis, MO 63130, 2004.

[19] Babuška I, Szabó BA, and Actis RL. Hierarchic models for laminated composites. *Int. J. Num. Meth. Engrg.*, 33:503–535, 1992.

[20] Naghdi PM. The theory of shells and plates. In S. Flügge, editor, *Encyclopedia of Physics*, pages 425–640. Springer-Verlag, Berlin, 1972.

[21] Novozhilov VV. *Thin Shell Theory.* P. Noordhoff Ltd., Groningen, 2nd edition, 1964.

[22] Actis R, Szabó B, and Schwab C. Hierarchic models for laminated plates and shells. *Comp. Methods Appl. Mech. Engrg.*, 172:79–107, 1999.

[23] Szabó B, Düster A, and Rank E. The p-version of the finite element method. In E. Stein, R. de Borst, and T. J. R. Hughes, editors, *Encyclopedia of Computational Mechanics*, volume Vol. 1, Chapter 5. John Wiley & Sons, Chichester, 2004.

[24] Babuška I and Strouboulis T. *The Finite Element Method and its Reliability.* Oxford University Press, Oxford, 2001.

[25] Clough RW and Tocher JL. Finite element stiffness matrices for analysis of plate bending. In *Proceedings of Conference on Matrix Methods in Structural Mechanics, Report AFFDL-TR-66-80*, pages 515–545. Wright-Patterson Air Force Base, Ohio, 1966.

[26] Greste O. Finite element analysis of tubular K joints. Technical Report UCSESM 70-11, University of California at Berkeley, June, 1970.

[27] Királyfalvi G and Szabó BA. Quasi-regional mapping for the p-version of the finite element method. *Finite Elem. Anal. Des.*, 27:85–97, 1997.

[28] Düster A, Bröker H, and Rank E. The p-version of the finite element method for three-dimensional curved thin walled structures. *Int. J. Num. Meth. Engrg.*, 52:673–703, 2001.

[29] Geymonat G and Sanchez-Palencia E. On the rigidity of certain surfaces with folds and applications to shell theory. *Arch. Rational Mech. Anal.*, 129:11–45, 1995.

[30] Oberkampf W. What are validation experiments? *Experimental Techniques*, pages 35–40, May/June 2001.

[31] Babuška I and Szabó B. On the Generalized Plane Strain Problem in Thermoelasticity, ICES Report 05-12, The University of Texas at Austin, Institute for Computational Engineering and Sciences, Austin, Texas, February 2005. Submitted for publication to *Comput. Methods Appl. Mech. Engng.*

REPORT DOCUMENTATION PAGE

AFRL-SR-AR-TR-05-

0155

1. AGENCY USE ONLY (Leave blank)	2. REPORT DATE 3/1/05	3. REPORT TYPE AND DATES COVERED Final Performance Report 12/1/00 to 11/30/2004

4. TITLE AND SUBTITLE
Mathematical and Computational Framework for Virtual Fabrication of Aircraft Structures

5. FUNDING NUMBERS
F49620-01-1-0074

6. AUTHOR(S)
Barna Szabó, Sebastian Nervi and Daniel Muntges

7. PERFORMING ORGANIZATION NAME(S) AND ADDRESS(ES)
Center for Computational Mechanics
Washington University, Box 1129
one Brookings Drive
St. Louis, MO 63130-4899

8. PERFORMING ORGANIZATION REPORT NUMBER
WUCCM-05-01

9. SPONSORING / MONITORING AGENCY NAME(S) AND ADDRESS(ES)
AFOSR
Attn: Fariba Fahroo-NM
875 North Randolph Street
Suite 325, Room 3112
Arlington VA 22203

10. SPONSORING / MONITORING AGENCY REPORT NUMBER

11. SUPPLEMENTARY NOTES

12a. DISTRIBUTION / AVAILABILITY STATEMENT
Approved for public release, Distribution Unlimited

12b. DISTRIBUTION CODE

13. ABSTRACT ***(Maximum 200 Words)***

The general objective of this project was to investigate the question of how working models should be formulated so that they can serve as reliable and accurate representations of physical reality in the sense that they will provide predictions of events or states of systems that can be confirmed consistently by physical observations. The construction of such mathematical models involves feedback processes, the main elements of which are calibration, prediction, evaluation and modification.

The specific objective was the development of the mathematical and computational aspects of a knowledge base needed for the creation of a virtual fabrication environment for aircraft components manufactured from 7050-T7451 aluminum plate stock so that the incidence of re-working and scrapping of partially or fully manufactured parts is substantially reduced.

The main conclusions are that verified mathematical models can be used successfully for the determination of residual stress states in 7050-T7451 aluminum plates and this information can be used for the prediction of distortion in thin-walled structural components with a high degree of reliability. The use of virtual and physical experiments in engineering decision-making processes is discussed and illustrated by examples.

14. SUBJECT TERMS			15. NUMBER OF PAGES
Mathematical models, verification, validation, virtual fabrication, residual stresses, dimensional reduction			16. PRICE CODE
17. SECURITY CLASSIFICATION OF REPORT U	18. SECURITY CLASSIFICATION OF THIS PAGE SAR	19. SECURITY CLASSIFICATION OF ABSTRACT SAR	20. LIMITATION OF ABSTRACT UU